Optimisation- vs. non-optimisation- based energy-maximising control for wave energy converters: A case study.

Nicolás Faedo[a], Demián García-Violini[b], Yerai Peña-Sanchez[a] and John V. Ringwood[a]

Abstract— Energy-maximising control of wave energy converters can be separated into two different classes: optimisation and non-optimisation based strategies. While optimisation-based controllers can outperform non-optimisation based strategies, the computational requirements associated with numerical optimisation routines, and the high control forces required under optimal conditions, can render these energy-maximising control laws unsuitable for realistic scenarios. Non-optimisation-based controllers present an alternative solution, where linear time-invariant systems are used to approximate the so-called *impedance-matching* condition. These strategies are often simple to implement but suffer from performance degradation when motion constraints are considered. This paper aims to present a critical comparison between both families of controllers, highlighting the strengths and weaknesses of each approach. We present simulation results for a state-of-the-art CorPower-like device under polychromatic (irregular) wave excitation, for both (motion) unconstrained and constrained scenarios.

I. Introduction

Energy-maximising control for wave energy converters (WECs) can be clearly divided into two categories: *optimisation-based* (OB) and *non-optimisation-based* (!OB) controllers (see, for example, [1]). In the case of optimisation-based controllers, the energy-maximising control objective is treated as an optimal control problem, where both input and state variables are often discretised using different criteria, aiming to map the infinite-dimensional problem into a computationally (numerically) tractable non-linear program, with model predictive control (MPC) as a typical example [2]. In contrast, non-optimisation-based controllers do not rely on numerical routines, but are mostly based on the fundamental principle behind maximum power transfer in electric circuits: the *impedance-matching* principle [3].

Naturally, OB and !OB come with clear differences, and each category presents its strengths and weaknesses. To be more precise, OB strategies compute an optimal control law u^{opt}, implemented through the so-called power take-off (PTO) system, by solving the *energy-maximising* optimal control formulation:

$$u^{\text{opt}} = \arg \max_{u \in \mathcal{U}} \frac{1}{T} \int_0^T v(t)u(t)dt, \qquad (1)$$
$$\text{subject to:} \begin{cases} \text{WEC dynamics,} \\ \text{state and input constraints,} \end{cases}$$

[a]Nicolás Faedo, Yerai Peña-Sanchez and John V. Ringwood are with the Centre for Ocean Energy Research, Maynooth University, Maynooth, Ireland `nicolas.faedo@mu.ie`
[b]Demián García-Violini is with Departamento de Ciencia y Tecnología, Universidad Nacional de Quilmes, Buenos Aires, Argentina.

where $T \in \mathbb{R}^+$, v denotes the velocity of the wave energy system and $\mathcal{U}$ denotes the set of admissible inputs. The optimal control formulation (1), which directly aims to maximise time-averaged power extraction from ocean waves, has been solved using a variety of strategies, mostly inspired by receding-horizon control techniques, such as MPC. An immediate advantage of this OB approach is that constraint handling becomes straightforward, *i.e.* one can translate physical limits on device motion and PTO force into state and input constraints in (1), as long as they represent a feasible set. A clear disadvantage is that the real-time capabilities of problem (1) depend on a number of factors, primarily the discretisation technique utilised to parameterise the state and input variables, and the hardware available for its implementation [1]. Examples can be found in[1], [4] (MPC), [5] (spectral optimal control) and [6], [7] (moment-based control).

On the other hand, !OB control strategies attempt to provide a (physically implementable) realisation of the impedance-matching condition for maximum power transfer. To be precise, under the assumption that there exists a frequency-response function G characterising the WEC dynamics, the impedance-matching condition explicitly utilises the so-called *intrinsic impedance* of the system, *i.e.* $Z = G^{-1}$, and the optimal control law that maximises power transfer (in the frequency-domain) can be shown [8] to be

$$U^{\text{opt}}(j\omega) = -Z^{\star}(j\omega)V(j\omega), \qquad (2)$$

where $\star : \mathbb{C} \to \mathbb{C}$ denotes the complex-conjugate operator, and U^{opt} and V denote the Fourier transform of u^{opt} and v, respectively. An immediate problem with (2) is that, as a direct consequence of the fact that the transfer function G is strictly proper, $Z^{\star}$ exhibits non-causal behaviour. In general, !OB control strategies attempt to find a realisable controller such that condition (2) holds, which is often obtained in terms of an approximating linear dynamical system. Another clear disadvantage of OB! strategies is that (2) does not observe any state nor input constraints, so that a different mechanism is required in the control loop to respect physical limitations associated with device and actuator dynamics. Despite such issues, !OB control techniques are popular within the wave energy community (particularly the industrial community), due to their computational efficiency, straightforward implementation and intuitive appeal. Examples of !OB can be found in [9], [10] and [11].

---

[1]The reader is referred to [1] for a comprehensive review of optimisation-based energy-maximising strategies.

This study aims to provide a critical comparison between two different strategies, each one representing the OB and !OB categories, both in terms of energy-maximising performance and applicability to realistic scenarios. The OB representative is a moment-based energy-maximising optimal control recently published in [6], [7]. This controller has the capabilities to effectively solve (1), guaranteeing existence and uniqueness of the optimal solution u^{opt}, with real-time performance. Within the !OB case, we select the linear time-invariant (LTI) controller presented in [11], which approximates condition (2) whilst providing a reliable (suboptimal) mechanism to handle motion constraints, making it suitable for realistic scenarios.

The remainder of this paper is organised as follows. Section II briefly recalls fundamentals behind modelling of WECs. Section III describes the moment-based OB control strategy, whilst Section IV discusses the LTI !OB controller. Section V presents a case study for a state-of-the-art CorPower-like device, where we provide a critical comparison between OB and !OB techniques in terms of performance and applicability to real scenarios. Finally, Section VI encompasses the main conclusions of this study.

A. Notation

Standard notation is used throughout this study with any exception detailed in this section. $\mathbb{R}^+$ ($\mathbb{R}^-$) denotes the set of non-negative (non-positive) real numbers. $\mathbb{C}^0$ denotes the set of pure-imaginary complex numbers. The symbol 0 stands for any zero element, dimensioned according to the context. The symbol $\mathbb{I}_n$ denotes the identity matrix of $\mathbb{C}^{n \times n}$. The spectrum of a matrix $A \in \mathbb{R}^{n \times n}$, *i.e.* the set of its eigenvalues, is denoted as $\lambda(A)$. The symbol $\bigoplus$ denotes the direct sum of n matrices, *i.e.* $\bigoplus_{i=1}^n A_i = \text{diag}(A_1, A_2, \ldots, A_n)$. The notation $\Re\{z\}$, with $z \in \mathbb{C}$, stands for the *real-part* operator. The *Kronecker product* between two matrices $M_1 \in \mathbb{R}^{n \times m}$ and $M_2 \in \mathbb{R}^{p \times q}$ is denoted by $M_1 \otimes M_2 \in \mathbb{R}^{np \times mq}$. The *Kronecker sum* between two matrices P_1 and P_2, with $P_1 \in \mathbb{R}^{n \times n}$ and $P_2 \in \mathbb{R}^{k \times k}$, is denoted as $P_1 \hat{\oplus} P_2$. The Fourier transform of a function f is denoted as F. Finally, the convolution between two functions f and g over $\mathbb{R}^+$ *i.e.* $\int_{\mathbb{R}^+} f(\tau)g(t-\tau)d\tau$, is denoted as $f * g$.

II. WEC MODELLING FUNDAMENTALS

The (linear) equation of motion for a 1 degree-of-freedom WEC can be expressed [8] as follows[2]:

$$m\ddot{x} = f_r + f_h + f_e - u, \qquad (3)$$

where m is the mass of the buoy, x the device excursion, f_e the wave excitation force (external input), f_h the hydrostatic restoring force, f_r the radiation force, and u the control (PTO) force. The linearised hydrostatic force can be written as $f_h(t) = -s_h x(t)$, where $s_h \geq 0$ denotes the hydrostatic stiffness. The radiation force f_r is modelled based on linear potential theory and, using the well-known Cummins'

equation [12], can be written as

$$f_r(t) = -\mu_\infty \ddot{x}(t) - \int_{\mathbb{R}^+} k(\tau)\dot{x}(t-\tau)d\tau, \qquad (4)$$

where $\mu_\infty = \lim_{\omega \to +\infty} \tilde{A}(\omega)$, $\mu_\infty > 0$, with $\tilde{A}(\omega)$ the radiation added mass[3], represents the added-mass at infinite frequency, and k is the (causal) radiation impulse response function. Finally, the equation of motion is given by

$$(m + \mu_\infty)\ddot{x} + k * \dot{x} + s_h x = f_e - u. \qquad (5)$$

Given that the LTI controller considered in Section IV intrinsically depends on the frequency-domain equivalent of (5), we note that the frequency-response mapping $G : \mathbb{C}^0 \to \mathbb{C}$ characterising the WEC dynamics, *i.e.* the operator G such

$$V(j\omega) = G(j\omega)\left[F_e(j\omega) - U(j\omega)\right], \qquad (6)$$

can be written as

$$G(j\omega) = \frac{j\omega}{s_h - \omega^2(m + \mu_\infty) + j\omega K(j\omega)}. \qquad (7)$$

Before discussing each particular control strategy, we note that the wave excitation force f_e is virtually always a non-measurable quantity. Consequently, estimation and forecasting strategies are usually required to effectively implement most of the energy-maximising controllers reported in the literature [13]. Though we explicitly declare the estimation/forecasting requirements of the OB and !OB strategies (and we use this as a comparative argument), we assume perfect knowledge of f_e in the case study of Section V, highlight the control performance differences, and rely on the spirit of the separation principle of control theory[4].

III. OB: MOMENT-BASED OPTIMAL CONTROLLER

The moment-based energy-maximising control strategy presented in [6], [7] provides an efficient and convenient way to parameterise the input and state variables in terms of the system-theoretic concept of *moment* (see [14]). Moments are intrinsically connected to the steady-state response characteristics of the system (WEC) under analysis, allowing for a parameterisation of problem (1) in terms of the steady-state response of a suitably defined interconnected system. Given the harmonic nature of ocean waves, [6], [7] the excitation force f_e and control input u are expressed as the solution of the *signal generator*

$$\dot{\xi} = S\xi, \quad f_e = L_e\xi, \quad u = L_u\xi, \qquad (8)$$

where the dynamic matrix $S \in \mathbb{R}^{\nu \times \nu}$ is such that $\lambda(S) = \{\pm p\omega_0\}_{p=1}^{\nu/2}$, with ν integer and even, and where ω_0 is the so-called *fundamental frequency* associated with the input variables f_e and u, *i.e.* $\omega_0 = 2\pi/T$. With the parameterisation of equation (8), and defining the following matrices

---

[2]From now on, we drop the dependence on $t \in \mathbb{R}^+$ when it is clear from the context.

[3]See [8] for the definition of $\tilde{A}(\omega)$.

[4]The effect of f_e estimation and forecasting errors has been documented elsewhere (e.g. [15]).

associated with the equation of motion (5):

$$A = \begin{bmatrix} 0 & 1 \\ -\dfrac{s_h}{m+\mu_\infty} & 0 \end{bmatrix}, \ B = \begin{bmatrix} 0 \\ \dfrac{1}{m+\mu_\infty} \end{bmatrix}, \ C^\mathsf{T} = \begin{bmatrix} 0 \\ 1 \end{bmatrix}, \tag{9}$$

the optimal control problem (1) can be mapped into a quadratic program (QP), *i.e.* the energy-maximising control input $u_{\mathrm{OB}}^{\mathrm{opt}} = L_u^{\mathrm{opt}}\xi$ can be computed as the unique global solution of the inequality-constrained concave quadratic optimisation problem

$$L_u^{\mathrm{opt}} = \arg\max_{L_u} -\frac{1}{2} L_u \Phi^{\mathscr{R}} L_u^\mathsf{T} + \frac{1}{2} L_e \Phi^{\mathscr{R}} L_u^\mathsf{T},$$

subject to: $\tag{10}$

$$\mathcal{A}_x L_u^\mathsf{T} \le \mathcal{B}_x, \quad \mathcal{A}_v L_u^\mathsf{T} \le \mathcal{B}_v, \quad \mathcal{A}_u L_u^\mathsf{T} \le \mathcal{B}_u,$$

where $\Phi^{\mathscr{R}} \in \mathbb{R}^{\nu\times\nu}$ explicitly contains both the WEC dynamics and input description as

$$\begin{aligned}\Phi^{\mathscr{R}} &= (\mathbb{I}_\nu \otimes C)\Phi^{-1}(\mathbb{I}_\nu \otimes -B),\\ \Phi &= S\,\hat{\oplus}\,A + \mathscr{R}^\mathsf{T} \otimes -BC.\end{aligned} \tag{11}$$

We note that the matrix $\mathscr{R} \in \mathbb{R}^{\nu\times\nu}$ characterises the non-parametric impulse response function k associated with radiation forces using moment-based theory, without the need to pre-compute a parametric approximation (which is the case for most of the OB methods reported in the literature [1]). The reader is referred to [6], [7] for the explicit definition of the operator $\mathscr{R}$, and the pairs of matrices $(\mathcal{A}_x, \mathcal{B}_x)$, $(\mathcal{A}_v, \mathcal{B}_v)$, $(\mathcal{A}_u, \mathcal{B}_u)$, which characterise displacement, velocity and control input constraints, respectively. Fig. 1 shows a block-diagram of the OB control architecture associated with (10).
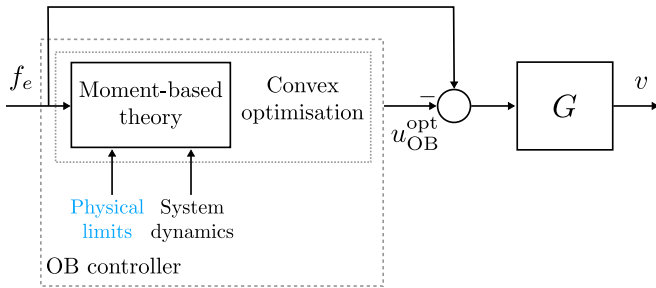

Fig. 1. Moment-based OB control structure. The physical limits are directly mapped into the moment-domain and added as inequality constraints to the optimisation problem. Note that perfect knowledge of f_e is assumed.

Given the concave nature of the QP expressed in (10), the optimal control force $u_{\mathrm{OB}}^{\mathrm{opt}}$ can be effectively computed in real-time, *i.e.* in less than one second (being consistent with the typical sampling rate of a full-scale WEC [6]). Nevertheless, we note that this optimal control formulation requires past, present and future knowledge of the wave excitation force f_e to compute the control law, and the associated estimation and prediction techniques naturally increase the overall computational demand.

IV. !OB: LTI CONTROLLER

As discussed in Section I, the !OB controller presented in [11] is based on the impedance-matching condition (2). Note that this controller is of an output feedback nature, which intrinsically complicates handling of motion constraints. Moreover, as analytically and numerical proven in [15], the closed-loop dynamics arising from (2) are extremely sensitive to variations in the (nominal) WEC dynamics G. Motivated by these issues, [11] presents an equivalent feedforward formulation of equation (2) expressed as

$$U^{\mathrm{opt}}(j\omega) = H_{\mathrm{ff}}(j\omega)F_e(j\omega), \tag{12}$$

where the optimal frequency-response function $H_{\mathrm{ff}} : \mathbb{C}^0 \to \mathbb{C}$ is given by

$$H_{\mathrm{ff}}(j\omega) = \frac{G(j\omega)}{2\Re\{G(j\omega)\}}. \tag{13}$$

This frequency-response mapping is approximated by a strictly proper and stable LTI system $\tilde{H}_{\mathrm{ff}} : \mathbb{C} \to \mathbb{C}$, using frequency-domain system identification techniques. We note that, as discussed in [11], H_{ff} does not correspond with any implementable transfer function, so that it is first necessary to define a frequency bandwidth in which to "focus" the identification technique. This frequency range is typically a function of the spectral characteristics of f_e.

Once the approximating LTI system $\tilde{H}_{\mathrm{ff}}$ is computed, the control structure (12) is modified to (suboptimally) observe constraints in the device motion:

$$U_{!\mathrm{OB}}^{\mathrm{opt}}(j\omega) = \left[\kappa\tilde{H}_{\mathrm{ff}}(j\omega) + (1-\kappa)\right]F_e(j\omega), \tag{14}$$

where $\kappa \in [0, 1]$. Fig. 2 illustrates the control structure defined in equation (14). The gain κ can be tuned adaptatively, using displacement and velocity measurements, or exploiting future knowledge of the wave excitation force (if available). We note that, in contrast to the OB controller, this strategy only requires wave excitation force estimation, obviating the need for a forecasting algorithm. This, however, has direct impact on the performance of the controller, as discussed in Section V.
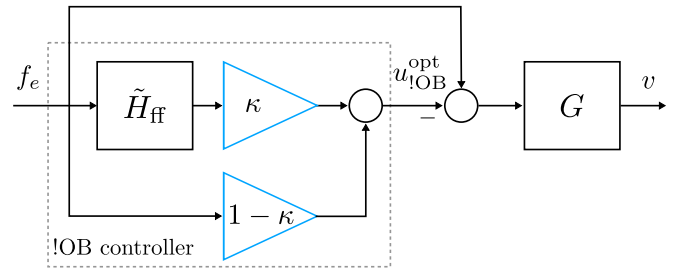

Fig. 2. LTI !OB control structure. The gain $\kappa \in [0\ 1]$ is used to handle motion constraints. Note that perfect knowledge of f_e is assumed.

V. CASE STUDY: A CORPOWER-LIKE DEVICE

This section presents a case study where we consider both OB and !OB control strategies applied to a state-of-the-art full-scale CorPower-like device oscillating in heave

(translational motion). This type of device is often considered as a case study due to its intrinsic geometric complexity (see, for example, [16]), and is illustrated in Fig. 3, with its corresponding physical dimensions specified in metres.
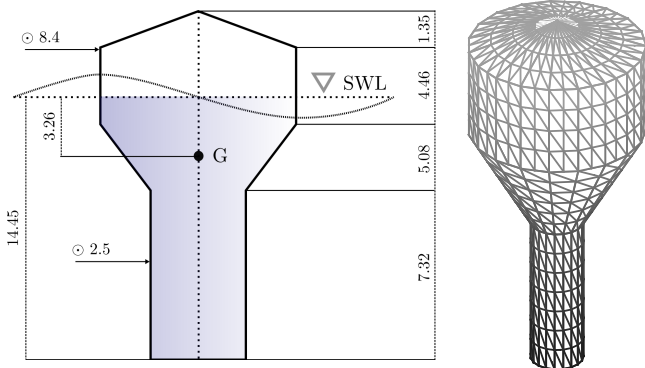

Fig. 3. Full-scale CorPower-like device considered in this case study. Dimensions are in metres. The acronym SWL stands for still water level and the letter **G** is used to denote the center of gravity of the device.

In the remainder of this section, we consider waves generated stochastically from a JONSWAP spectrum [17], with a fixed significant wave height H_s of 2 [m], peak period $T_p \in [5, 12]$ [s], peak shape parameter $\gamma = 3.3$, and time-length of 120 [s]. To be statistically consistent, the results presented in the following paragraphs are always averaged over 20 realisations of each sea-state considered. Finally, we note that the controller *normalised run-time*, *i.e.* the ratio between the time required to compute the optimal control input for the duration of the simulation, and the length of the simulation itself, is used as a comparison metric for the computational effort required by each strategy. The computations are performed using MATLAB 2018b, running on a PC composed of an *Intel Xeon CPU E5-1620 processor* with 16 GB of RAM.

As discussed in Section IV, the !OB controller requires a linear system $\tilde{H}_{\text{ff}}$ approximating condition (12). To compute such a system, we utilise the moment-based identification strategy presented in [18]. Fig. 4 illustrates the optimal frequency-response H_{ff} (dashed-black), computed directly from the hydrodynamic response of the CorPower-like device, and the frequency-response of the approximating model $\tilde{H}_{\text{ff}}$ (solid-green). The white area in Fig. 4 indicates the frequency range selected (containing all possible peak periods of the generated waves) to perform the identification process, *i.e.* $[0.3, 3]$ [rad/s]. The order (dimension) of $\tilde{H}_{\text{ff}}$, for this case study, is set to 14, corresponding to seven interpolation frequencies (see [18]).

A. Unconstrained control

As a preliminary step, we start the comparison between OB and !OB controllers by analysing the unconstrained control problem, *i.e.* energy-maximisation *without* considering any physical limitations. For the OB controller, this is equivalent to solving (10) ignoring state and input constraints, while, for the !OB controller, the gain κ is set to 1.
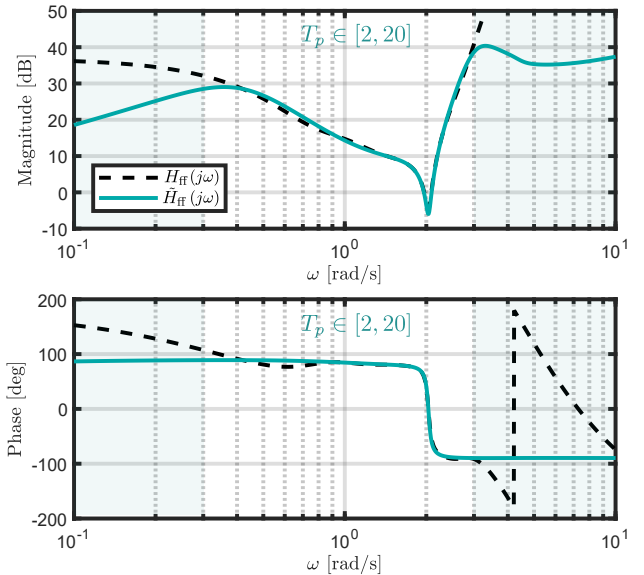

Fig. 4. Optimal frequency-response H_{ff} (dashed-black) computed directly from the hydrodynamic response of the CorPower-like device, and the frequency-response of the approximating model $\tilde{H}_{\text{ff}}$ (solid-green). The white area indicates the frequency range selected for identification, covering wave peak periods in the range $[2, 20]$.

Fig. 5 presents absorbed power results for each of the sea-states considered. It can be appreciated that the impedance-matching condition of the !OB controller captures almost the same power as the OB controller for peak periods < 10 [s]. The drop in performance after $T_p = 10$ [s], *i.e.* when $\omega_p < 0.62$ [rad/s], can be attributed to the decrease in approximation quality of $\tilde{H}_{\text{ff}}$ in such a frequency region. We also highlight that the computational effort required by both strategies is similar, as can be appreciated in Table I.
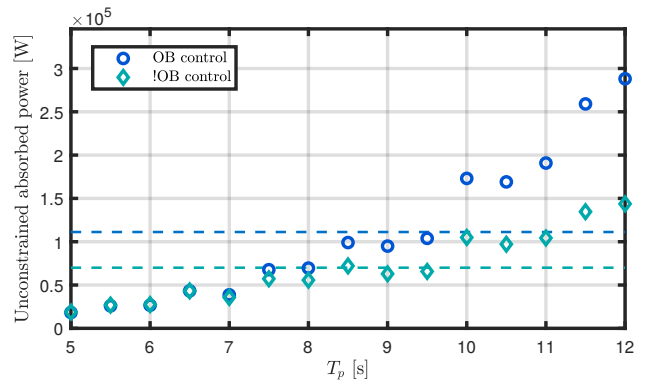

Fig. 5. Unconstrained power absorption for OB ($\circ$) and !OB ($\diamond$) controllers. The dashed -blue and -green lines indicate the average power extracted for the totality of the sea-states considered, for OB and !OB cases, respectively.

B. Constrained control

We now analyse a more realistic scenario, where we constrain the displacement of the device to the operational space $[-2, 2]$ [m]. We note that the LTI !OB controller does not handle constraints in an independent manner, but rather utilises a single gain to tune displacement, velocity and

	Controller	Average power over $T_p \in [5, 12]$	Average max. control input over $T_p \in [5, 12]$	Normalised run-time
Unconstrained	**OB**	0.11×10^6 [W]	3.6×10^6 [N]	30.5×10^{-6} [s]
	!OB	0.07×10^6 [W]	2.4×10^6 [N]	28.1×10^{-6} [s]
Constrained in x	**OB**	0.06×10^6 [W]	1.1×10^6 [N]	2.1×10^{-4} [s]
	!OB	0.02×10^6 [W]	0.8×10^6 [N]	28.1×10^{-6} [s]

maximum control input simultaneously. However, in turn, the OB controller solves a constrained optimisation problem.

Fig. 6 presents results for the constrained scenario, for each of the sea-states considered. In the case of the !OB controller, the gain κ is optimally (iteratively) tuned for each wave, using perfect knowledge of the excitation force, guaranteeing that the displacement of the WEC is contained within the maximum limits during the complete simulation. Unlike the unconstrained case of Section V-A, the drop in performance experienced by the !OB controller is now more evident: This can be strictly attributed to the suboptimal constraint handling mechanism, *i.e.* the constant gain κ, which, for sea-states with $T_p > 7$ [s], cannot fully capture the energy-maximising optimality condition. This is not the case for the moment-based OB controller, which can incorporate displacement constraints in a straightforward manner, using the pair of matrices $(\mathcal{A}_x, \mathcal{B}_x)$ in equation (10). The difference in constraint handling between OB and !OB controllers can be fully appreciated in Fig. 7, where time-traces of displacement for irregular waves of $T_p = 6$ [s] (top) and $T_p = 10$ [s] (bottom) are explicitly shown. When $T_p = 6$ [s], the motion of the device is similar for both OB and !OB controllers, which corresponds with the similarity in extracted power for that particular wave peak period, as can be appreciated from Fig. 6. On the contrary, when $T_p = 10$ [s], the motion of the device under optimal control conditions is much more likely to hit the maximum displacement limit, and the suboptimal constraint handling of the !OB controller compromises performance. This can be appreciated in Fig. 7 (bottom) where, in contrast to the !OB controller, the moment-based OB control strategy fully exploits the operational space $[-2, 2]$ [m], resulting in considerably higher power extraction.

However, the superior energy-capturing performance of the OB controller comes with (potential) drawbacks. Firstly, even though achieving real-time performance in the test PC, the normalised run-time required by the OB controller is two orders of magnitude greater than that for the !OB case (see Table I), which can be limiting for realistic applications, where its successful implementation depends upon available software/hardware. Secondly, as can be appreciated from Fig. 8 and Table I, the (average) maximum control force required by the OB controller is $\approx 70\%$ larger than for the !OB LTI strategy, which has a direct impact on the design of the PTO system [19]. In addition, the high-frequency content of the OB control signal may have an adverse effect on device/component lifetime. Note that the maximum PTO
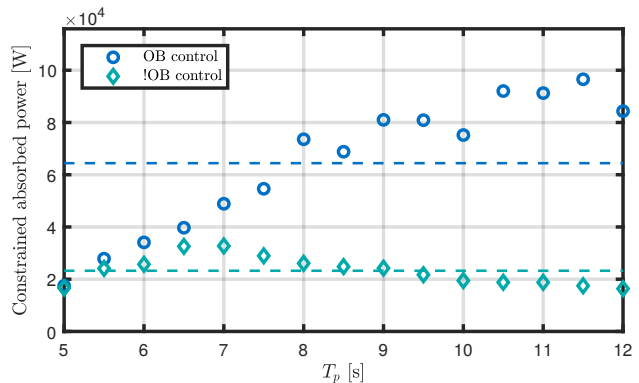

Fig. 6. Constrained power absorption for OB (○) and !OB (◇) controllers. The dashed -blue and -green lines indicate the average power extracted for the totality of the sea-states considered, for OB and !OB cases, respectively.
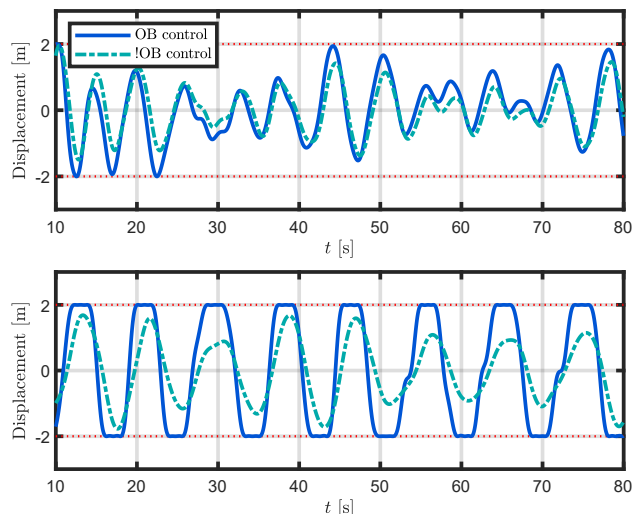

Fig. 7. Time-traces of device displacement, for irregular waves of $T_p = 6$ [s] (top) and $T_p = 10$ [s] (bottom). The dotted-red lines indicate the physical limits considered in metres.

force required directly influences the size of the PTO system, regardless of the technology selected: a larger maximum PTO force requires larger hydraulic pistons or higher pressure in hydraulic PTO system [20], while greater maximum PTO forces require larger machines in linear generators [21]. Though beyond the scope of this study, maximum PTO force constraints can be incorporated in the OB case using the pair of matrices $(\mathcal{A}_u, \mathcal{B}_u)$, to mitigate large control forces.

Even if computational power and large PTO forces are available in the actual control implementation, there is one clear recommendation that arises naturally from this section:

if this CorPower-like WEC is located in a particular geo-graphic area characterised by peak periods between 5 and 7 seconds, the !OB controller represents a wiser choice, being able to extract similar power figures as the OB controller, with mild computational requirements and smaller control forces. If peak periods are greater than 7 seconds, the OB controller becomes a more suitable alternative, starting to outperform the !OB strategy significantly, hence representing a major improvement in terms of power absorption.
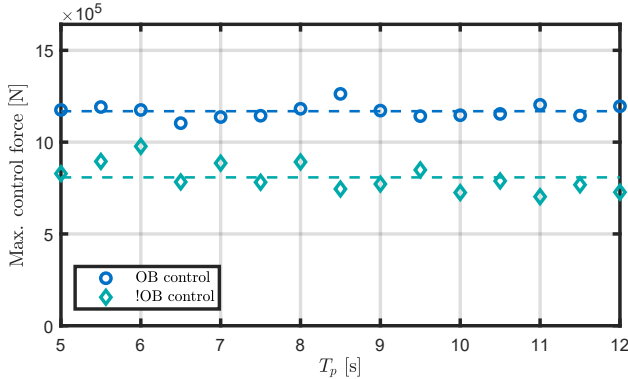

Fig. 8. Maximum control force required by OB ($\circ$) and !OB ($\diamond$) controllers for the constrained case. The dashed -blue and -green lines indicate the average max. control force for the totality of the sea-states considered, for OB and !OB cases, respectively.

VI. CONCLUSIONS

This study compares two different energy-maximising control strategies, representing optimisation-based and non-optimisation-based control solutions, and provides a set of recommendations on whether to consider OB or !OB strate-gies depending on PTO characteristics and hardware/soft-ware available for real-time control implementation.

Though suboptimal in terms of power performance, the !OB controller studied is synthesised as an LTI system, which is simple to implement, with mild computational require-ments, and offering some intuitive appeal. The constraint mechanism is composed of a constant gain, which can be easily tuned to respect physical limits associated with a real device. Unsurprisingly, the more sophisticated moment-based OB controller outperforms the !OB strategy in terms of power absorption, especially in the constrained scenario. Nevertheless, this increase in performance comes with higher PTO forces and computational requirements, which could be potentially limiting in real scenarios.

We conclude that OB control strategies are suitable when specialised hardware is available to solve constrained opti-misation in real-time, and when high control forces can be handled by the PTO system utilised. If the control imple-mentation is limited in terms of computational power and/or the PTO system cannot deal with high control forces, !OB control strategies are a more suitable candidate, providing acceptable power extraction with mild requirements. Finally, in the case where both computational power and high PTO forces are available, a wise controller selection can be achieved as a function of the location where the device is

intended to be deployed: some sea-states, until reaching a (device-dependent) critical peak period, can be effectively handled almost optimally with an !OB controller, whilst a considerable gain in power absorption can be achieved with OB control after this critical point.

REFERENCES

[1] N. Faedo, S. Olaya, and J. V. Ringwood, "Optimal control, MPC and MPC-like algorithms for wave energy systems: An overview," *IFAC Journal of Systems and Control*, vol. 1, pp. 37–56, 2017.

[2] ——, "Optimal control, mpc and mpc-like algorithms for wave energy systems: An overview," *IFAC Journal of Systems and Control (Peer-Review)*, vol. 1, 2017.

[3] T. L. Floyd and E. Pownell, *Principles of electric circuits*. Prentice Hall, 1997.

[4] G. Li and M. R. Belmont, "Model predictive control of sea wave energy converters–part i: A convex approach for the case of a single device," *Renewable Energy*, vol. 69, pp. 453–463, 2014.

[5] G. Bacelli and J. V. Ringwood, "Numerical optimal control of wave energy converters," *IEEE Transactions on Sustainable Energy*, vol. 6, no. 2, pp. 294–302, 2015.

[6] N. Faedo, G. Scarciotti, A. Astolfi, and J. V. Ringwood, "Energy-maximising control of wave energy converters using a moment-domain representation," *Control Engineering Practice*, vol. 81, pp. 85 – 96, 2018.

[7] ——, "Moment-based constrained optimal control of an array of wave energy converters," in *2019 American Control Conference (ACC), Philadelphia*, 2019, pp. 4797–4802.

[8] J. Falnes, *Ocean waves and oscillating systems: linear interactions including wave-energy extraction*. Cambridge university press, 2002.

[9] R. H. Hansen, "Design and control of the power take-off system for a wave energy converter with multiple absorbers," Ph.D. dissertation, Aalborg University, Aalborg, Denmark, 2013.

[10] F. Fusco and J. V. Ringwood, "A simple and effective real-time con-troller for wave energy converters," *IEEE Transactions on sustainable energy*, vol. 4, no. 1, pp. 21–30, 2012.

[11] D. García-Violini, Y. Peña-Sanchez, N. Faedo, and J. V. Ringwood, "An energy-maximising linear time invariant controller (LiTe-Con) for wave energy devices," *Submitted to IEEE Transactions on sustainable energy*, 2019.

[12] W. Cummins, "The impulse response function and ship motions," DTIC Document, Tech. Rep., 1962.

[13] Y. Peña-Sanchez, M. Garcia-Abril, F. Paparella, and J. V. Ringwood, "Estimation and forecasting of excitation force for arrays of wave energy devices," *IEEE Transactions on Sustainable Energy*, 2018.

[14] A. Astolfi, "Model reduction by moment matching for linear and nonlinear systems," *IEEE Transactions on Automatic Control*, vol. 55, no. 10, pp. 2321–2336, 2010.

[15] J. V. Ringwood, A. Mérigaud, N. Faedo, and F. Fusco, "An analytical and numerical sensitivity and robustness analysis of wave energy control systems," *IEEE Transactions on Control Systems Technology (early access available)*, 2019.

[16] G. Giorgi and J. V. Ringwood, "Analytical representation of nonlinear froude-krylov forces for 3-dof point absorbing wave energy devices," *Ocean Engineering*, vol. 164, pp. 749–759, 2018.

[17] K. Hasselmann, "Measurements of wind wave growth and swell decay during the Joint North Sea Wave Project (JONSWAP)," *Dtsch. Hydrogr. Z.*, vol. 8, p. 95, 1973.

[18] N. Faedo, Y. Peña-Sanchez, and J. V. Ringwood, "Finite-order hy-drodynamic model determination for wave energy applications using moment-matching," *Ocean Engineering*, vol. 163, pp. 251 – 263, 2018.

[19] M. Penalba and J. Ringwood, "A review of wave-to-wire models for wave energy converters," *Energies*, vol. 9, no. 7, p. 506, 2016.

[20] R. Hansen, M. Kramer, and E. Vidal, "Discrete displacement hydraulic power take-off system for the wavestar wave energy converter," *Energies*, vol. 6, no. 8, pp. 4001–4044, 2013.

[21] J. Cruz, *Ocean wave energy: current status and future prespectives*. Springer Science & Business Media, 2007.